

# Crystal Plasticity Modeling for FCC Metals

Hui Zhou

Department of Materials Science and Engineering,  
City University of Hong Kong, Kowloon, Hong Kong, China  
(Dated: Aug, 2022)

## I. INTRODUCTION

Structure materials are essential to construct automobiles, airplanes and ships. Their performances, such as strength and toughness, play important roles in the safety, reliability and fuel-efficiency of these transportation vehicles. Among all the structure materials, metal and alloys are the primary materials in load-carrying body and engine components. Increasing fuel-efficiency can be achieved directly by increasing the engine combustion conditions [1] or weight reduction of these structure components, which in turn requires increases in their mechanical performances.

The mechanical performance of metal and alloys are largely determined by the generation, evolution and interaction of crystal defects such as dislocation, twin, grain and interface boundaries. For example, the yield strengths of most metals and alloys follow the Hall-Petch relation where strength increases with reduction of microstructure length scales such as grain sizes. Increasing strength can thus be achieved via microstructure refinement, which however, almost always leads to reductions in other properties such as tensile ductility. In practice, the microstructure length scales are thus chosen to achieve the best overall properties of the material.

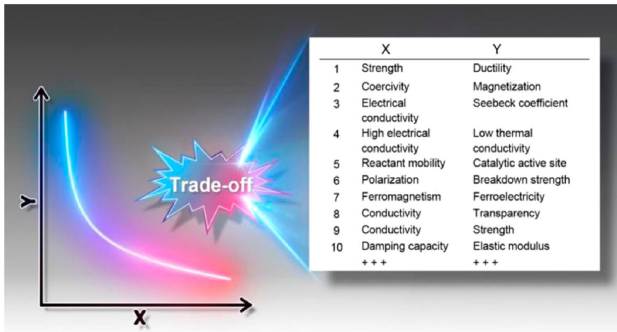


Figure 1: Inverse relationships among material properties following the “banana” envelop. (Figure from Ref. [2])

Microstructure engineering has been pursued for more than a century while most alloys still have strength-ductility limited by the “banana shape” envelop (Fig. 1 and Ref. [2]). Emerging heterogeneous structured materials, such as those with bimodal grain sizes [3] or harmonic microstructures [4] (Fig. 2), are recently shown to break the “banana shape” envelop, resulting in both superior strength and ductility not achievable by conventional alloys. In these materials, plastic deformation is highly complex. The underlying mechanisms include dislocation and twin interactions with grain boundaries, interfaces, precipitations, and possibly solid-solutions. However, these mechanisms operate at different scales and deformation stages, interact with each other, and are not well understood.

Figure 3 shows an example of a steel processed by a SPEX mill [2]. This material exhibits a gradient-structured with grains of nanometer sizes at the surface and coarse grains underneath the surface towards the center. In addition, the surface microstructure has a strong texture in the  $\langle 110 \rangle$  and  $\langle 111 \rangle$  directions. The texture weakens in deeper sections. In this gradient-structured material, the surface layer has relatively high strength due to its nanogranined microstructure based on the Hall-Petch relation, while the inner layers with large grain sizes are softer. The plastic deformation is thus highly complex with influences

from the varying grain sizes and texture.

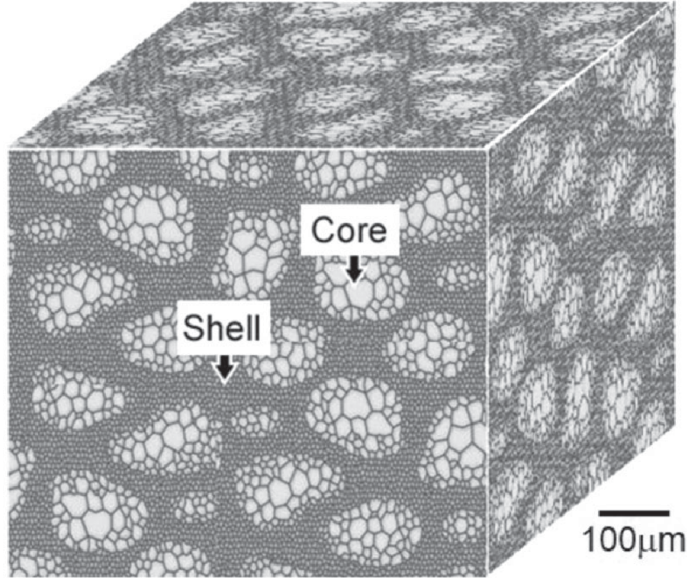


Figure 2: 3D illustration of a harmonic structured material consisting of coarse soft grains and ultrafine hard grains. (Figure from Ref. [2])

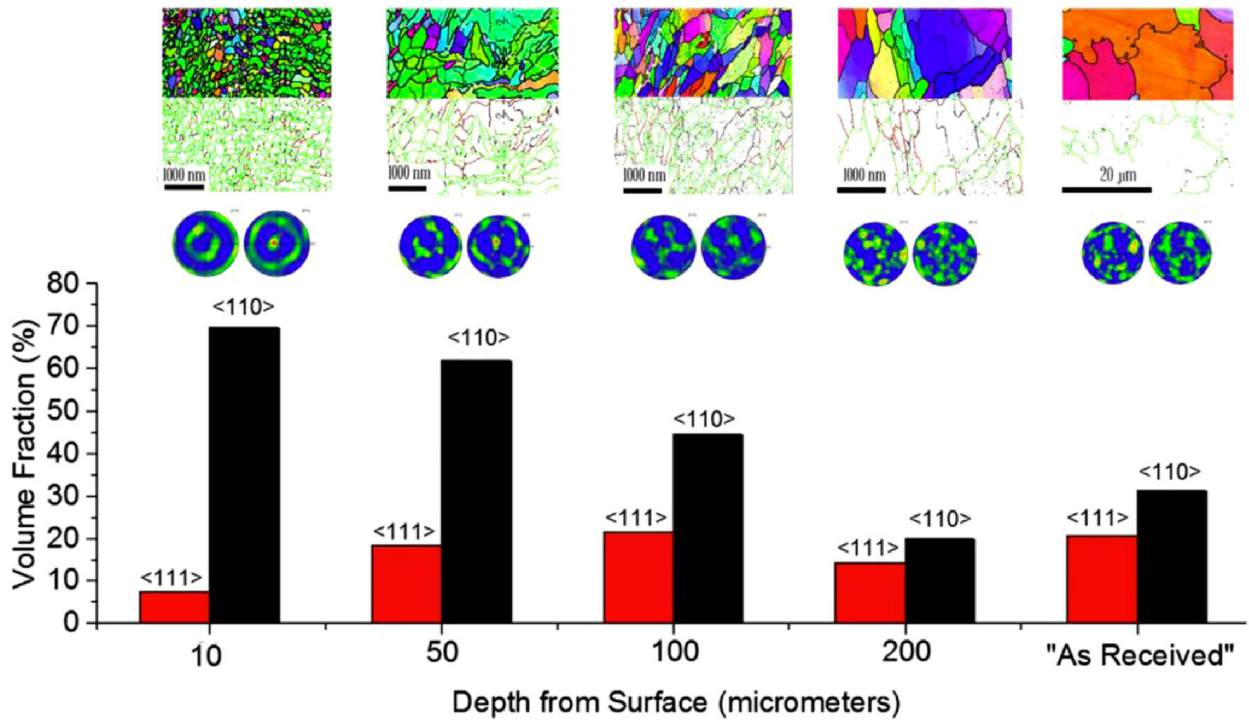


Figure 3: Grain size and orientation as a function of depth from the surface of a gradient-structured steel processed using a SPEX Mill. (Figure from Ref. [2])

In heterogeneous structured materials, plastic deformation is characterized by (i) nonuniform plastic strain partitioning in the plastically “soft” and “hard” regions (e.g., nano and

coarse grains in Fig. 2); (ii) strong interactions of dislocations with microstructure interfaces and (iii) heterogeneous forward and back stresses resulting from strain gradient near interfaces. Figure 4 illustrates the forward and back stress in heterogeneous structured materials.

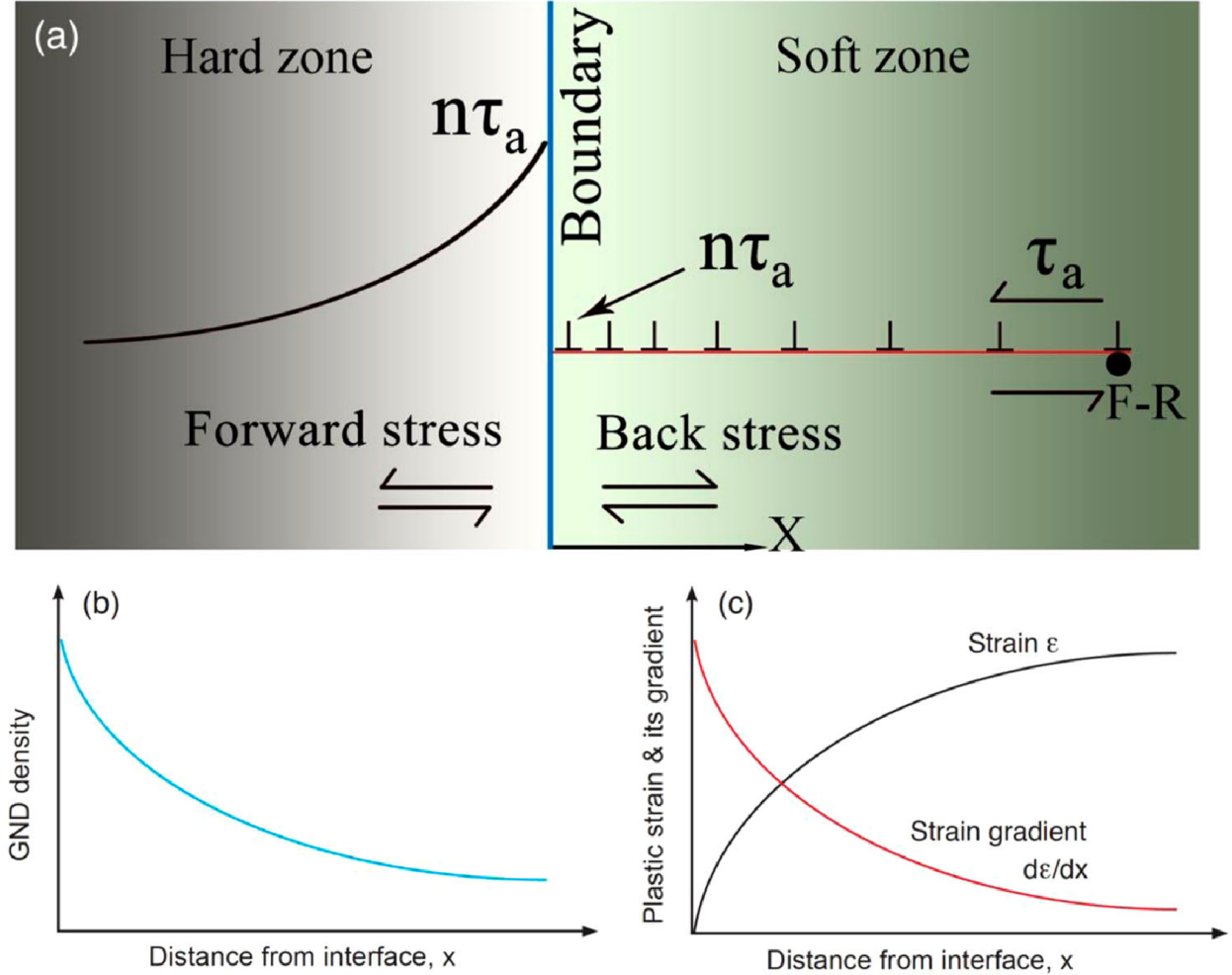


Figure 4: Dislocation pile-ups with forward and back stresses at interfaces. (a) An applied shear stress  $\tau_a$  causes a GND pile-up emitted from a Frank-Read dislocation source. In the soft zone, the dislocation pile-ups generates a back stress and induces the forward stress in the hard zone. At the boundary, the stress is amplified to  $\sim n\tau_a$ , where the  $n$  is number of dislocations in the pile-ups. (b) GND density in the pile-ups as a function of distance from the boundary. (c) Plastic strain and strain gradient as a function of distance from the boundary. (Figure from Ref. [2])

Heterogeneous structured materials derive their unique properties from nonhomogeneous plastic slip in the interface regions, which essentially is characterized by dislocation pile-ups. Figure 4 illustrates a dislocation pile-ups at a boundary under applied shear stress  $\tau_a$ . The dislocation pile-ups is known as the geometrically necessary dislocation (GND [5]). Its

density is related to the plastic strain gradient as [6],

$$\rho_{\text{GND}} = \frac{1}{b} \frac{\partial \gamma_{\text{pl}}}{\partial x}, \quad (1)$$

where  $b$  is the Burgers vector and  $\gamma_{\text{pl}}$  is the plastic shear strain. The Taylor model [7] gives the relation of local flow stress  $\tau_{\text{loc}}$  and statistically stored dislocation (SSD) density  $\rho_s$  as

$$\tau_{\text{loc}}(x) = \alpha G b \sqrt{\rho_s(x)}, \quad (2)$$

where  $\alpha$  is a prefactor and  $G$  is the shear modulus. Mughrabi shows that under constant total strain, the plastic strain gradient  $\frac{\partial \gamma_{\text{pl}}}{\partial x}$  can be related to the elastic strain gradient  $\frac{\partial \gamma_{\text{el}}}{\partial x}$ , which in turn relates  $\rho_{\text{GND}}$  to the  $\rho_s$  as [8],

$$\rho_{\text{GND}}(x) = -\frac{\alpha}{2\sqrt{\rho_s}} \frac{\partial \rho_s}{\partial x}. \quad (3)$$

The force acting on a dislocation is the Peach-Koehler [9] force

$$\mathbf{f} = (\boldsymbol{\sigma} \cdot \mathbf{b}) \times \boldsymbol{\xi}, \quad (4)$$

where  $\boldsymbol{\sigma}$  is the stress tensor and  $\boldsymbol{\xi}$  is the dislocation line direction. In the dislocation pile-ups, the leading dislocation thus experiences a force per unit length

$$f_1 = \sum_{i=2}^n (\boldsymbol{\sigma}_i \cdot \mathbf{b}) \times \boldsymbol{\xi} + (\boldsymbol{\sigma}_{\text{a}} \cdot \mathbf{b}) \times \boldsymbol{\xi} \quad (5)$$

where  $\boldsymbol{\sigma}_i$  is the stress generated by dislocation  $i$  and the summation includes all dislocations (except the leading one) in the pile-ups (Fig. 5). In the hard and soft zones, the forward and back stresses are essentially the summation of dislocation self-stresses plus the applied stress

$$\boldsymbol{\sigma}_{\text{back/forward}}(\mathbf{x}) = \sum_{i=1}^n \boldsymbol{\sigma}_i + \boldsymbol{\sigma}_{\text{a}}. \quad (6)$$

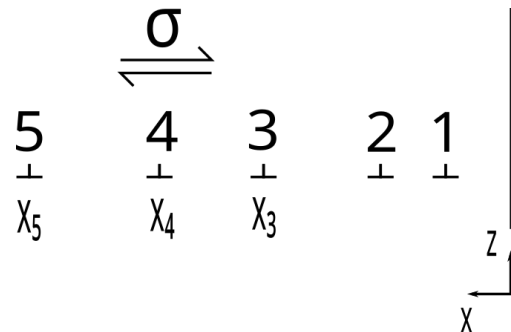


Figure 5: Edge dislocations piled up at a grain boundary. (Fig.21-1 from Hirth [10])

In Fig. 4, if the pile-ups is taken as a superdislocation [10], the force acting on the leading dislocation per unit length can be written as

$$\frac{F}{L} = n\tau_a b. \quad (7)$$

This force is balanced by the resistance created at the boundary due to change of slip system or slip discontinuity. The resistance can be thought of a lattice friction at the boundary. At sufficiently high  $\sigma_a(\tau_a)$  and/or pile-ups size  $n$ , the driving force can be higher than the resistance and the leading dislocation can cross the boundary, which may initiates macro yielding or plastic flow.

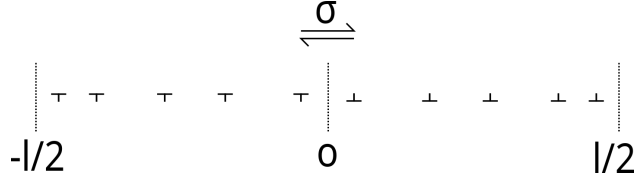


Figure 6: Edge dislocation pileup forms by a Frank-Read source at the center of the interval. (Fig.21-4 from Hirth [10])

The backstress of the dislocation pileup can be obtained from Chapter 21 in Hirth [10] (Fig. 6). Firstly, the dislocation density is derived from the equilibrium of the externally applied stress and internally dislocation pileup,

$$\sigma b = \frac{\mu b^2}{2\pi(1-\nu)} \int_{-l/2}^{l/2} \frac{n(x')dx'}{x' - x}, \quad -\frac{l}{2} \leq x \leq \frac{l}{2} \quad (8)$$

where the dislocation density  $n(x) = \pm \frac{1}{b} \frac{db}{dx}$  that is the number of the dislocations per length. Thus, the dislocation density can be obtained in the following,

$$n(x) = \frac{2(1-\nu)\sigma}{\mu b} \frac{x}{\sqrt{(l/2)^2 - x^2}} \quad (9)$$

where  $l$  is the length of double pileup,  $\mu$  is shear modulus,  $\nu$  is the Poisson's ratio and  $\sigma$  is the externally applied stress. The  $x < 0$  part of the Eq. 9 corresponds to the blue curve in the (b) part of Fig. 4.

The total number  $N$  of dislocations in the pileup of either sign is

$$N = \int_0^{l/2} n(x)dx = \frac{(1-\nu)l\sigma}{\mu b} \quad (10)$$

the total shear strain  $\varepsilon$ , by integrating the disregistry in the pileup, is

$$\varepsilon = \int_{-\frac{l}{2}}^x bx'n(x')dx' \quad (11)$$

Substitute the Eq. 10 into the Eq. 11,

$$\varepsilon(x) = \frac{(1-\nu)\sigma}{\mu} \left(\frac{l}{2}\right)^2 \left[ \arcsin \frac{2x}{l} + \frac{\pi}{2} - \frac{2x}{l} \sqrt{1 - \left(\frac{2x}{l}\right)^2} \right] \quad (12)$$

thus the total shear strain

$$\varepsilon = \varepsilon(l/2) = \frac{\pi(1-\nu)l^2\sigma}{4\mu} \quad (13)$$

the Burgers vector cancels out in Eq. 13, the continuum approximation for the pileup is equivalent to a shear crack. The  $x < 0$  part of the Eq. 12 and its derivative  $d\varepsilon/dx$  corresponds to the red curve in the (c) part of Fig. 4.

Finally, the backstress from a superdislocation  $Nb$ , according to the Hirth [10] (Ch. 21, Eq. 21-36),

$$\sigma_{\text{back}} = \frac{l\sigma}{2x} = \frac{\mu Nb}{2\pi(1-\nu)x} \quad (14)$$

which has the  $1/x$  asymptotics corresponds to the black curve in the (a) part of Fig. 4.

The dislocation slip and twinning are the main plastic deformation mode of metals. For dislocation slip, the quantity Burgers vector  $b$  is a fraction of lattice vector  $a$ . The Burgers vector is the same order of the lattice vector if applies for twinning. The volume fraction  $f$  in  $[0, 1]$  is used to quantify the twinned region and untwinned region. Dislocation slips contributed to the stage I (easy-glide) deformation and twinnings the stage II deformation in the three-stage stress-strain curve. In Cheng et al. [11], the volume fraction of twinning is included in their crystal plasticity model and agrees with the stage II deformation from experiments. The plastic strain or deformation is accumulation of individual dislocation activities: glide, cross-slip, interaction with themselves, interaction with solutes and grain boundaries. The higher the SSD density the harder to move the GND in turns the higher yielding strength. Moreover, the higher the SSD density the smaller the untwinned region in turns the higher cross-slip strength as well. In Kords's thesis [12], the non-local dislocation density model takes account of dislocation density transport was first developed.

The crystal plasticity theory used the microstructure length scale or the dislocation density as a kind of grain coarsening and included the grain size, orientation and composite effects as a refinement of the continuum mechanics. It exhibited the material anisotropy and linked directly to the experimental observations. In the following chapters, the Hooke's law will be reviewed and the fundamentals of crystal plasticity will be explained.

## II. HOOKE'S LAW

The Hooke's law of elasticity theory is written in terms of stress and strain in the following

$$\sigma_{ij} = C_{ijkl}\varepsilon_{kl} \quad (15)$$

where the  $C_{ijkl}$  are elastic constants,  $\sigma_{ij}$  is the Cauchy stress and  $\varepsilon_{kl}$  is the infinitesimal strain, i.e.,  $\varepsilon_{kl} = \frac{1}{2}(u_{k,l} + u_{l,k})$ . The elastic moduli  $C_{ijkl}$  are also denotes the  $\mathcal{L}$  later in the crystal plasticity notation.

The Cauchy stress is symmetric due to the conservation of angular momentum,

$$\sigma_{ij} = \begin{bmatrix} \sigma_{11} & \sigma_{12} & \sigma_{13} \\ \sigma_{21} & \sigma_{22} & \sigma_{23} \\ \sigma_{31} & \sigma_{32} & \sigma_{33} \end{bmatrix} \quad (16)$$

The elastic constants  $C_{ijkl}$  has the following symmetry properties in general

$$C_{ijkl} = C_{jikl} = C_{ijlk} = C_{klij} \quad (17)$$

Consider the symmetry of lattice structures, for example, the  $x_1 - x_2$  is the reflection plane, then the elastic constants are reduced to (Ch. 13-4, Eq. 13-97 in Hirth [10]),

$$C_{ijkl} = \begin{bmatrix} c_{11} & c_{12} & c_{13} & 0 & 0 & c_{16} \\ c_{12} & c_{22} & c_{23} & 0 & 0 & c_{26} \\ c_{13} & c_{23} & c_{33} & 0 & 0 & c_{36} \\ 0 & 0 & 0 & c_{44} & c_{45} & 0 \\ 0 & 0 & 0 & c_{45} & c_{55} & 0 \\ c_{16} & c_{26} & c_{36} & 0 & 0 & c_{66} \end{bmatrix} \quad (18)$$

Following the same arguments, the cubic crystal has three nonzero elastic constants  $c_{11} = c_{22} = c_{33}$ ,  $c_{12} = c_{13} = c_{23}$ ,  $c_{44} = c_{55} = c_{66}$ . The Voigt average of elastic constants (Ch. 13-2, Eq. 13-26 in Hirth [10]) are

$$\lambda + 2\mu = c_{11} + \frac{2}{5}H \quad (19)$$

$$\mu = c_{44} - \frac{1}{5}H \quad (20)$$

$$\lambda = c_{12} - \frac{1}{5}H \quad (21)$$

where  $H = 2c_{44} + c_{12} - c_{11}$  is the anisotropy factor. The quadratic form of elastic energy requires that  $6 \times 6$  matrix  $C_{ijkl}$  is positive definite, which is called Born stability criteria [13]. For cubic crystal,

$$c_{11} > 0, \quad c_{11} + 2c_{12} > 0, \quad c_{44} > 0. \quad (22)$$

Thus, the elastic moduli matrix is invertible,

$$\varepsilon_{ij} = S_{ijkl}\sigma_{kl}. \quad (23)$$

It is noted that the  $9 \times 9$  matrix  $C_{ijkl}$  can not be inverted as its  $6 \times 6$  version (Ch. 13-2, Eq. 13-11 in Hirth [10]).

### III. FINITE STRAIN THEORY

The deformation gradient is defined as in Fig. 7,

$$\mathbf{F} = \frac{\partial \mathbf{x}}{\partial \mathbf{X}} \quad (24)$$

where  $\mathbf{X}$  represents the reference configuration  $\Omega_0$  and  $\mathbf{x}$  represents the current configuration  $\Omega$ . Hence, the deformation gradient is a Jacobian matrix of  $x(X, t)$  with the determinant  $J = \det(\mathbf{F}) > 0$ . The reference configuration is a stress-free state.

The deformation gradient in this definition has the polar decompostion

$$\mathbf{F} = \mathbf{R}\mathbf{U} = \mathbf{V}\mathbf{R} \quad (25)$$

where  $\mathbf{R}$  is rotation matrix,  $\mathbf{U}$  and  $\mathbf{V}$  are right and left stretch matrices respectively.

The Green deformation tensor is defined as

$$\mathbf{C} = \mathbf{F}^T \mathbf{F} \quad (26)$$

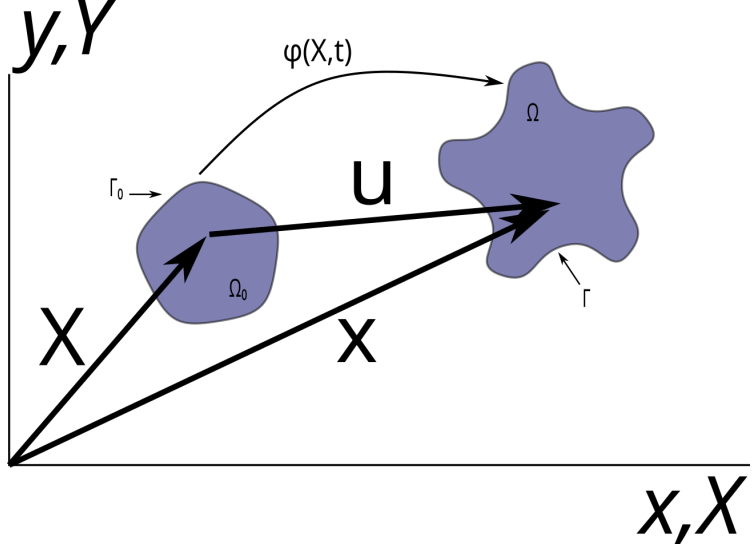


Figure 7: A continuum body deformed by a mapping  $x = \phi(X, t)$  where  $X \in \Omega_0$  and  $x \in \Omega$ ,  $\Gamma_0$  and  $\Gamma$  are their boundaries. Figure 3.1 from Belytschko [14].

and the Lagrangian strain is defined as

$$\mathbf{E} = \frac{1}{2} (\mathbf{C} - \mathbf{I}) \quad (27)$$

they are used to measure the strain in the reference configuration  $\Omega_0$ .

The velocity gradient is defined as

$$\mathbf{L} = \frac{\partial \mathbf{v}}{\partial \mathbf{x}} = \frac{\partial \mathbf{v}}{\partial \mathbf{X}} \frac{\partial \mathbf{X}}{\partial \mathbf{x}} = \dot{\mathbf{F}} \mathbf{F}^{-1} \quad (28)$$

where  $\dot{\mathbf{F}}$  is the time derivative of deformation gradient. Its symmetric part is the strain rate and anti-symmetric part is the spin tensor,

$$\mathbf{D} = \text{sym}(\mathbf{L}) = \frac{1}{2} (\mathbf{L} + \mathbf{L}^T) \quad (29)$$

$$\mathbf{W} = \text{asym}(\mathbf{L}) = \frac{1}{2} (\mathbf{L} - \mathbf{L}^T) \quad (30)$$

In the crystalline material particularly face-centred cubic (FCC) crystals, the deformation mechanisms are due to dislocation slip and twinning. In order to model these behaviors, the deformation gradient is decomposed as

$$\mathbf{F} = \mathbf{F}^{\text{el}} \mathbf{F}^{\text{pl}} \quad (31)$$

where  $\mathbf{F}^{\text{el}}$  is the elastic part with property  $\det(\mathbf{F}^{\text{el}}) = J$  and  $\mathbf{F}^{\text{pl}}$  is the plastic part with property  $\det(\mathbf{F}^{\text{pl}}) = 1$ .

Substitute the Eq. 31 into the Eq. 28, the velocity gradient becomes

$$\begin{aligned} \mathbf{L} &= \dot{\mathbf{F}}^{\text{el}} (\mathbf{F}^{\text{el}})^{-1} + \mathbf{F}^{\text{el}} \left[ \dot{\mathbf{F}}^{\text{pl}} (\mathbf{F}^{\text{pl}})^{-1} \right] (\mathbf{F}^{\text{el}})^{-1} \\ &= \mathbf{L}^{\text{el}} + \mathbf{F}^{\text{el}} \mathbf{L}^{\text{pl}} (\mathbf{F}^{\text{el}})^{-1} \end{aligned} \quad (32)$$

The plastic velocity gradient  $\mathbf{L}^{\text{pl}}$  in Eq. 32 consists of the shear strain rate on the slip systems,

$$\mathbf{L}^{\text{pl}} = \sum_{\alpha=1}^n \dot{\gamma}^\alpha \mathbf{m}^\alpha \otimes \mathbf{n}^\alpha \quad (33)$$

where the summation index  $\alpha$  goes through all the active slip systems.  $\mathbf{m}^\alpha$  is the slip direction and  $\mathbf{n}^\alpha$  is the slip plane normal.  $\dot{\gamma}$  is the shear rate. According to the Orowan's equation,

$$\dot{\gamma} = \rho_m b v \quad (34)$$

the shear rate is characteristic of the mobile dislocations. The velocity of the dislocations  $v$  is proportional to the applied stress however limited to the speed of sound. The Schmid factor  $\mathbf{m}^\alpha \otimes \mathbf{n}^\alpha$  represents the crystallographic orientation of slip plane. The lattice vectors  $\mathbf{m}$  and  $\mathbf{n}$  are deformed in the intermediate configuration. Substitute the Eq. 33 into the Eq. 32,

$$\mathbf{m}^{*(\alpha)} = \mathbf{F}^{\text{el}} \mathbf{m}^\alpha \quad (35)$$

$$\mathbf{n}^{*(\alpha)} = (\mathbf{F}^{\text{el}})^{-T} \mathbf{n}^\alpha \quad (36)$$

Take the time derivative of both sides and use the lattice deformation rate,

$$\dot{\mathbf{m}}^{*(\alpha)} = \mathbf{L}^{\text{el}} \mathbf{m}^{*(\alpha)} \quad (37)$$

$$\begin{aligned} \dot{\mathbf{n}}^{*(\alpha)} &= (\mathbf{L}^{\text{el}})^{-T} \mathbf{n}^{*(\alpha)} \\ &= -(\mathbf{L}^{\text{el}})^T \mathbf{n}^{*(\alpha)} \end{aligned} \quad (38)$$

We illustrated here a simple shear case, the elastic deformation gradient is given as

$$\mathbf{F}^{\text{el}} = \begin{bmatrix} 1 & \delta \\ 0 & 1 \end{bmatrix} \quad (39)$$

the elastic deformation rate is accordingly

$$\mathbf{L}^{\text{el}} = \dot{\mathbf{F}}^{\text{el}} (\mathbf{F}^{\text{el}})^{-1} = \begin{bmatrix} 0 & \dot{\delta} \\ 0 & 0 \end{bmatrix} \quad (40)$$

then,  $\mathbf{m} = [1, 0]$  maps to  $\mathbf{m}^* = [1, 0]$  and  $\mathbf{n} = [0, 1]$  maps to  $\mathbf{n}^* = [0, 1]$ . In the infinitesimal case, the shear strain is

$$\gamma = \frac{\delta}{d} \quad (41)$$

where  $d$  is the spacing of two atomic planes. We have known that the shear stress will move the dislocations and cause the slips. As the slip occurs, the dislocations will move out of the body until the surface is reached. This procedure will, as a result, decrease the spacing  $d$  and the quantity strain is amplified to capture the infinitesimally small transverse movement. On the unloading, the elastic shear strain is given as

$$\gamma_e = \frac{\tau_c}{G} \quad (42)$$

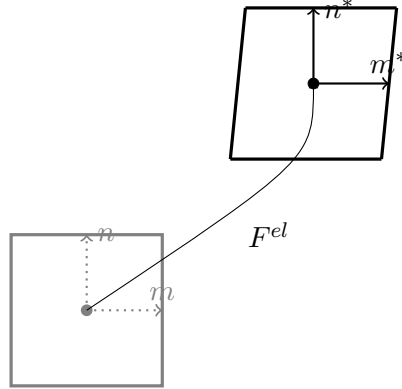


Figure 8: The lattice did not stretch or rotate in the simple shear case (the elastic deformation gradient  $\mathbf{F}^{\text{el}}$  in Eq. 39 with  $\delta = 0.1$ .)

where  $G$  is the shear modulus. Since the strain hardening is achieved, the critical resolved shear stress  $\tau_c$  is greater than the initial shear stress  $\tau_0$ . The gauge of the transverse movement is increased in the end.

In comparison with the plastic strain, the elastic strain is negligible and the material is nearly incompressible. The plastic deformations as an irreversible process are rather due to shear stress than pressure. Therefore, the approximation  $\mathbf{L} \approx \mathbf{L}^{\text{pl}}$  is usually used without loss of generality.

Though the plastic deformation gradient  $\mathbf{F}^{\text{pl}}$  has the property  $\det(\mathbf{F}^{\text{pl}}) = 1$ . The rotation matrix is excluded from  $\mathbf{F}^{\text{pl}}$ . In other words, the polar decomposition of  $\mathbf{F}^{\text{pl}}$  is not fulfilled. Therefore, the  $\mathbf{F}^{\text{pl}}$  is unsymmetric. The matrix in terms of hyperbolic function fulfills this criterion, in particular, the sech and the tanh functions.

As an example, the  $\mathbf{F}^{\text{pl}}$  can be written as follows,

$$\mathbf{F}^{\text{pl}} = \begin{bmatrix} \operatorname{sech}(x) & \tanh(x) \\ -\tanh(x) & \operatorname{sech}(x) \end{bmatrix} \quad (43)$$

which is unsymmetric and the  $\det(\mathbf{F}^{\text{pl}}) = 1$ . The deformation mapping of the  $\mathbf{F}^{\text{pl}}$  is depicted in Fig. 9.

The plastic velocity gradient is therefore

$$\mathbf{L}^{\text{pl}} = \dot{\mathbf{F}}^{\text{pl}} (\mathbf{F}^{\text{pl}})^{-1} = \dot{x} \begin{bmatrix} 0 & \operatorname{sech}(x) \\ -\operatorname{sech}(x) & 0 \end{bmatrix} \quad (44)$$

which means  $\mathbf{L}^{\text{pl}} = \mathbf{W}^{\text{pl}}$ . The invariant of matrix  $\det(\mathbf{L}^{\text{pl}}) = [\dot{x}\operatorname{sech}(x)]^2$ .

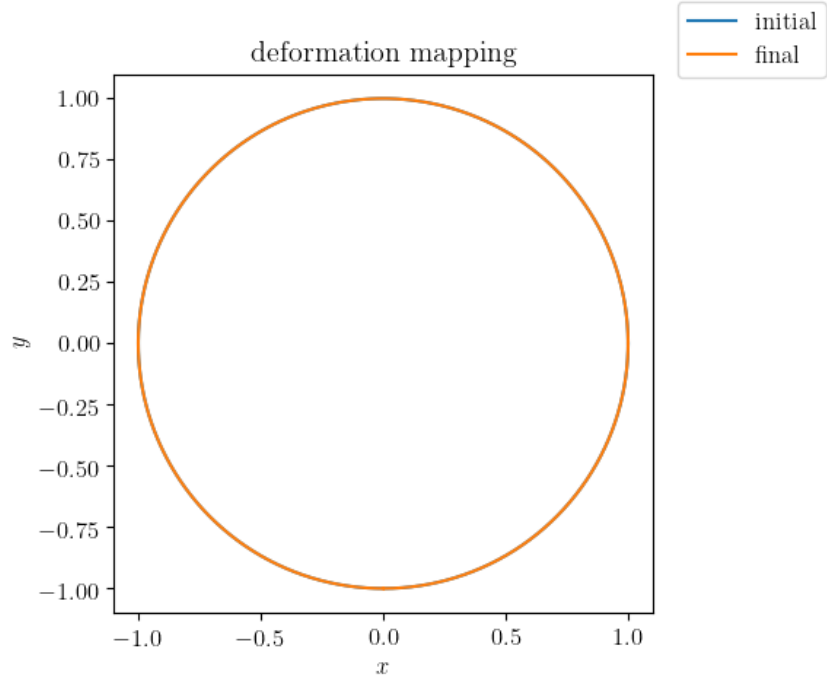
The Cauchy stress of pure shear is

$$\boldsymbol{\sigma} = \begin{bmatrix} 0 & \tau \\ \tau & 0 \end{bmatrix} \quad (45)$$

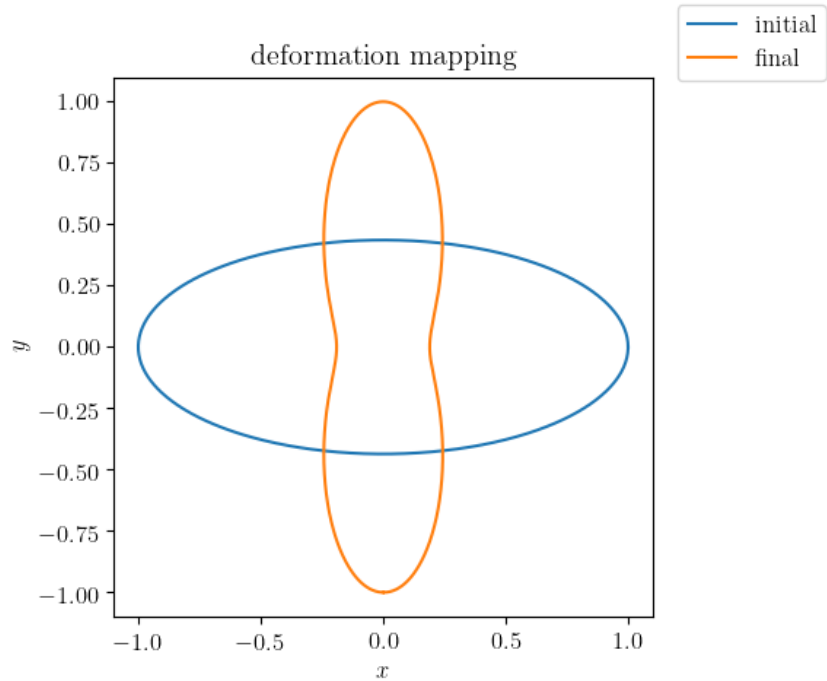
The work rate per unit volume  $\boldsymbol{\sigma} : \mathbf{L}^{\text{pl}} = 0$  showing that this is the perfect plastic modeling.

If the strain rate energy is assumed as

$$\begin{aligned} w^{\text{pl}} &= \frac{\alpha}{2} [\det(\mathbf{L}^{\text{pl}})] \\ &= \frac{\alpha}{2} \{[\dot{x}\operatorname{sech}(x)]^2\} \end{aligned} \quad (46)$$



(a) A circle mapped by the  $\mathbf{F}^{\text{pl}}$  in Eq. 43 overlaps itself



(b) An ellipse mapped by the  $\mathbf{F}^{\text{pl}}$  in Eq. 43 excludes the rotation

Figure 9: The two properties of the plastic deformation gradient. 9a) volume-preserving.  
9b) rotation exclusion.

where  $\alpha$  is constant. The energetic stress conjugate to  $\dot{x}$  is

$$\tau_c = \frac{\partial w^{\text{pl}}}{\partial \dot{x}} = \alpha \dot{x} \operatorname{sech}^2(x) \quad (47)$$

For crystals, the variable of  $\mathbf{F}^{\text{pl}}$  is the shear strain  $\gamma$ . Eq. 47 is reformulated as a critical resolved shear stress (crss) function

$$\tau_c = \alpha \dot{\gamma} \operatorname{sech}^2(\gamma) \quad (48)$$

In Eq. 48, the conjugate (viscous) stress is proportional to shear strain rate initially and become rate-independent after a small amount of shear strains are accumulated. The constant  $\alpha$  has the unit of viscosity. The initial crss or the slip yield stress  $\tau_0 = \alpha \dot{\gamma}$  is essential in crystal plasticity modeling because it represents the turning point of dilatent to distortion plastic behavior.

#### IV. SLIP HARDENING MODEL

The constitutive law of  $\dot{\gamma}^\alpha$  in Eq. 33 employs the viscoplastic power-law relation in literature,

$$\dot{\gamma}^\alpha = \dot{\gamma}_0 \left( \frac{\tau^\alpha}{g^\alpha} \right)^n \quad (49)$$

where  $\dot{\gamma}_0$  is a reference strain rate,  $n$  is the rate sensitivity exponent and  $g^\alpha$  is the slip resistance of the  $\alpha$ th system. The reformulation of Eq. 49,

$$\begin{aligned} \tau^\alpha(\gamma) &= g^\alpha(\gamma) \left( \frac{\dot{\gamma}^\alpha}{\dot{\gamma}_0} \right)^{\frac{1}{n}} \\ \gamma &= \sum_{\beta=1}^N \int_0^t |\dot{\gamma}^\beta| dt \end{aligned} \quad (50)$$

is the constitutive law of shear stress-strain in the  $\alpha$ th slip system.  $\gamma$  is the total plastic strain of all the slip systems representing the plastic deformation history. The shear stress becomes rate-independent if  $n$  takes a large value ( $\geq 20$ ).

The initial slip resistance  $g^\alpha(0)$  is the crss of the  $\alpha$ th slip system. Its interaction with other slip systems is given by the hardening rate,

$$\dot{g}^\alpha = \sum_{\beta=1}^N h_{\alpha\beta} \dot{\gamma}^\beta \quad (51)$$

The theoretical shear strength of slip  $\tau_{\text{th}} = G/2\pi$  is many orders magnitude larger than the crss due to dislocations [15]. Asaro and Needleman [16] proposed the following viscoplastic model in which the hardening evolution is assigned for each slip system rather than a critical threshold stress.

$$h(\gamma) = h_0 \operatorname{sech}^2 \left( \frac{h_0 \gamma}{\tau_s - \tau_0} \right) \quad (52)$$

The constant  $h_0$  represents an initial hardening rate and  $\tau_s$  denotes a saturation strength.  $\tau_0$  is the initial strength for each slip system  $\alpha$ .

Fig. 10b showed the slip systems in FCC lattice structures. Each half edge represents a slip direction and triangle a slip plane/normal. Considering the slip interaction, the Bassani-Wu model [17] has the following form,

$$\begin{aligned} h_{\alpha\alpha} &= F(\gamma_\alpha)G(\{\gamma_\beta; \beta = 1, N, \beta \neq \alpha\}) \quad (\text{no sum on } \alpha), \\ h_{\beta\alpha} &= qh_{\alpha\alpha}, \alpha \neq \beta \quad (\text{no sum on } \alpha), \\ F(\gamma_\alpha) &= \{(h_0 - h_s)\operatorname{sech}^2\left[\frac{(h_0 - h_s)\gamma_\alpha}{\tau_s - \tau_0}\right] + h_s\}, \\ G(\{\gamma_\beta; \beta = 1, N, \beta \neq \alpha\}) &= 1 + \sum_{\beta=1, \beta \neq \alpha}^N f_{\alpha\beta} \tanh(\gamma_\beta/\gamma_0) \end{aligned} \quad (53)$$

In the single slip hardening function  $F(\gamma_\alpha)$ ,  $\tau_0$  is the initial critical resolved shear stress,  $\tau_s$  is the stage I stress or the breakthrough stress where large plastic flow initiates,  $h_0$  is the hardening modulus just after initial yield, and  $h_s$  is the hardening modulus during easy glide. The latent hardening coefficient  $q$  takes value  $1.0 \sim 1.4$ .

In the slip interaction function  $G(\{\gamma_\beta; \beta = 1, N, \beta \neq \alpha\})$ ,  $\gamma_0$  is the amount of slip after which the interaction between slip system  $\alpha$  and  $\beta$  reaches peak strength. Here, for simplicity,  $\gamma_0$  is taken to be the same [ $\gamma_0 = (\tau_s - \tau_0)/h_0$ ] for all pairs of systems and each component  $f_{\alpha\beta}$  represents the magnitude of the strength of a particular slip interaction.

Chapter 9-5 FCC Metals in Hirth [10] states the large number of possible choices of slip systems for polycrystals of FCC metals. In contrast, an uniaxial tension done in Fig. 10a shows only three slip systems (three curves: 1, 2, 10) are activated. This observation is coped with continuum theory. We take the Thompson tetrahedron from Figure 9-15 in Hirth [10] for illustration, the unit cell in Fig. 11 is typical in theory of elasticity where the stress components are defined on each faces. The crystal plasticity further divides this cell into the tetrahedron that has four faces. If one of the four faces is where the external forces are applied, the other three faces are activated by the shear stress. Therefore, we usually pick three slip systems to characterize the shear deformation for single crystal. In fact, the deviatoric strain has the three off-diagonal terms ( $\varepsilon'_{12}, \varepsilon'_{13}, \varepsilon'_{23}$ ) that the crystal plasticity is furnishing.

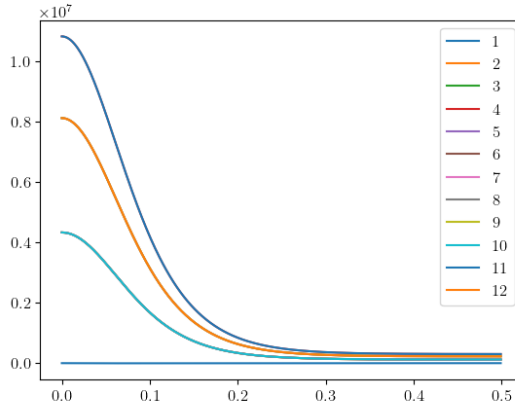
## V. OBJECTIVE STRESS RATE

For large deformations involving the rotation of slip plane, the Cauchy stress defined in the current configuration is pulled back to the reference configuration using the deformation mapping. As the coordinate system is rotated, the Hooke's law is thus modified by the objective stress rate on the left hand side and the deformation rate of that system on the right hand side.

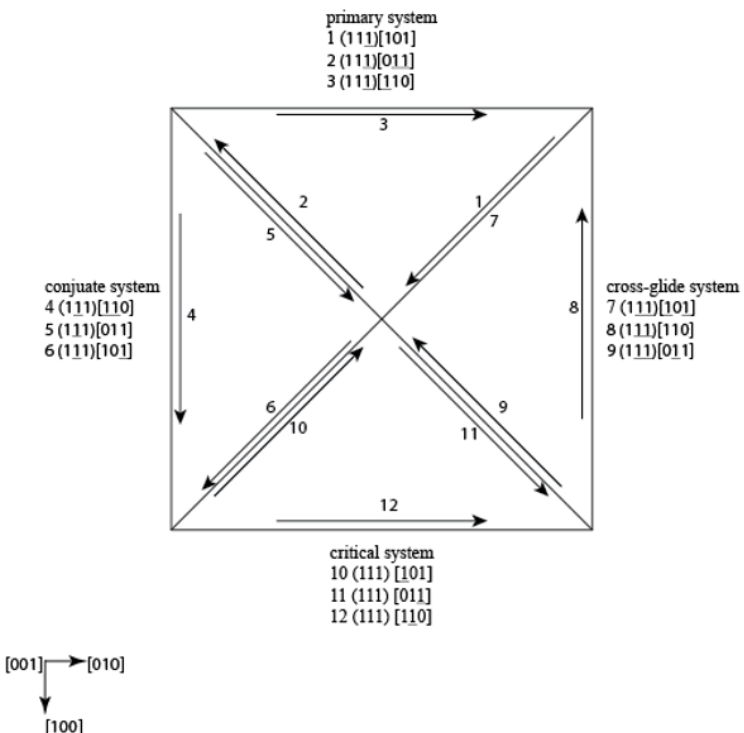
In the reference configuration, the second Piola-Kirchhoff stress is used instead of the Cauchy stress. The second Piola-Kirchhoff stress is work conjugate to the Lagrangian strain defined as

$$\mathbf{S} = J\mathbf{F}^{-1}\boldsymbol{\sigma}\mathbf{F}^{-T} \quad (54)$$

where  $\boldsymbol{\sigma}$  is the Cauchy stress and  $\boldsymbol{\tau} = J\boldsymbol{\sigma}$  is the Kirchhoff stress.



(a)



(b)

Figure 10: 10a glide hardening rates of Bassani model [17]. The slip of the 1st direction in primary system interacts with the 2nd direction (coplanar junction) and the 10th direction in critical system (Hirth lock), which shows that these slip systems are active. 10b FCC lattice slip systems are composed of the primary system, conjugate system, cross-glide system and critical system.

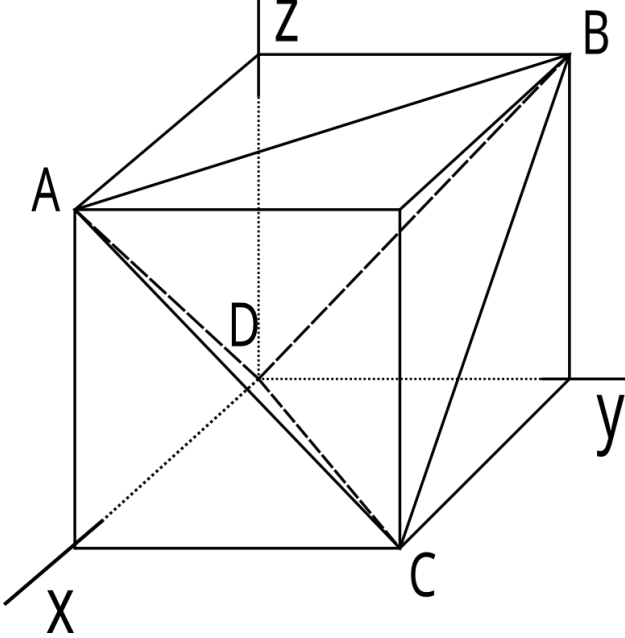


Figure 11: A unit cell in the fcc lattice with an enclosed tetrahedron, the faces of which are the possible glide planes and the edges of which are the possible glide directions. Figure 9-15 from Hirth [10]

The Truesdell rate of the Cauchy stress is defined as

$$\check{\sigma} = \dot{\sigma} - \mathbf{L}\sigma - \sigma\mathbf{L}^T + \text{Tr}(\mathbf{L})\sigma \quad (55)$$

The Jaumann rate of the Cauchy stress is defined as

$$\check{\sigma} = \dot{\sigma} + \sigma\mathbf{W} - \mathbf{W}\sigma \quad (56)$$

which is used here in the finite element program.

The Mandel stress tensor is defined to be

$$\begin{aligned} \mathbf{M} &= \mathbf{C}\mathbf{S} \\ &= J\mathbf{F}^T\sigma\mathbf{F}^{-T} \end{aligned} \quad (57)$$

which is often used to describe inelastic (plastic) materials. The Mandel stress tensor is in general not symmetric and defined with respect to an intermediate configuration. Using polar decomposition  $\mathbf{F} = \mathbf{R}\mathbf{U}$ ,

$$\begin{aligned} \mathbf{M} &= J\mathbf{F}^T\sigma\mathbf{F}^{-T} \\ &= J\mathbf{U}(\mathbf{R}^T\sigma\mathbf{R})\mathbf{U}^{-1} \end{aligned} \quad (58)$$

The intermediate configuration is an inelastic configuration. The rate of the Mandel stress is

$$\dot{\mathbf{M}} = J\mathbf{F}^T[\dot{\sigma} + \sigma\text{Tr}(\mathbf{L}) + \mathbf{L}^T\sigma - \sigma\mathbf{L}^T]\mathbf{F}^{-T} \quad (59)$$

which can be approximated by taking  $\mathbf{F} = \mathbf{F}^{\text{el}}$  and  $\mathbf{L} = \mathbf{D}^{\text{el}}$ .

$$\dot{\mathbf{M}} = J(\mathbf{F}^{\text{el}})^T[\dot{\sigma} + \sigma\text{Tr}(\mathbf{D}^{\text{el}}) + \mathbf{D}^{\text{el}}\sigma - \sigma\mathbf{D}^{\text{el}}](\mathbf{F}^{\text{el}})^{-T} \quad (60)$$

The term  $[\dot{\sigma} + \sigma \text{Tr}(\mathbf{D}^{\text{el}}) + \mathbf{D}^{\text{el}}\sigma - \sigma\mathbf{D}^{\text{el}}]$  contributed to the inelastic deformation.

The projection of Mandel stress rate on the slip plane  $\mathbf{m}^\alpha \otimes \mathbf{n}^\alpha$

$$\begin{aligned}\dot{\tau}_n^m &= \dot{\mathbf{M}} : \mathbf{m}^\alpha \otimes \mathbf{n}^\alpha \\ &= [\dot{\sigma} + \sigma \text{Tr}(\mathbf{D}^{\text{el}}) + \mathbf{D}^{\text{el}}\sigma - \sigma\mathbf{D}^{\text{el}}] : (\mathbf{F}^{\text{el}}\mathbf{m}^\alpha) \otimes (\mathbf{F}^{\text{el}})^{-T} J \mathbf{n}^\alpha\end{aligned}\quad (61)$$

which shows that the  $(\mathbf{F}^{\text{el}}\mathbf{m}^\alpha)$  is in the deformed configuration and the  $(\mathbf{F}^{\text{el}})^{-T} J \mathbf{n}^\alpha$  is in the reference configuration. Thus, the Mandel stress tensor, similar to the first Piola-Kirchhoff stress tensor  $\mathbf{P}$ , is unsymmetric and is a two-point tensor.

The work-conjugate relations of stress and strain are

$$\mathbf{S} : \dot{\mathbf{E}} = \boldsymbol{\tau} : \mathbf{L} = \mathbf{P} : \dot{\mathbf{F}} = \mathbf{M} : \mathbf{F}^{-1} \dot{\mathbf{F}} \quad (62)$$

the strain rate  $\mathbf{l} = \mathbf{F}^{-1} \dot{\mathbf{F}}$  conjugate to the Mandel stress. Therefore, the Hooke's law can be applied in the rate form.

$$\dot{\mathbf{M}} = \mathcal{C} : \mathbf{l} \quad (63)$$

where  $\mathcal{C}$  is the fourth-order elastic moduli. We shall derive the Cauchy stress-strain rate relation by substituting Eq. 63 into Eq. 59,

$$\begin{aligned}J\mathbf{F}^T \dot{\sigma} \mathbf{F}^{-T} &= \mathcal{C} : \mathbf{l} - \mathbf{M} \text{Tr}(\mathbf{l}) - \mathbf{l}^T \mathbf{M} + \mathbf{M} \mathbf{l}^T \\ \dot{\sigma} : \mathbf{F} \mathbf{m} \otimes J\mathbf{F}^{-T} \mathbf{n} &= [(\mathcal{C} - \mathbf{M} \otimes \mathbf{I}) : \mathbf{l} - \mathbf{l}^T \mathbf{M} + \mathbf{M} \mathbf{l}^T] : \mathbf{m} \otimes \mathbf{n} \\ \dot{\sigma} : \mathbf{F} \mathbf{m} \otimes J\mathbf{F}^{-T} \mathbf{n} &= [(\mathcal{C} - \mathbf{M} \otimes \mathbf{I}) : \mathbf{m} \otimes \mathbf{n} - (\mathbf{m} \otimes \mathbf{n})^T \mathbf{M} + \mathbf{M} (\mathbf{m} \otimes \mathbf{n})^T] : \mathbf{l}\end{aligned}\quad (64)$$

Introducing the elasticity moduli tensor transformation [13]  $\mathcal{C} - \mathbf{M} \otimes \mathbf{I} = J\mathbf{F}^T \mathcal{L} \mathbf{F}^{-T}$ ,

$$\begin{aligned}\dot{\sigma} : \mathbf{F} \mathbf{m} \otimes J\mathbf{F}^{-T} \mathbf{n} &= \\ [\mathcal{L} : \mathbf{F} \mathbf{m} \otimes J\mathbf{F}^{-T} \mathbf{n} - (\mathbf{F} \mathbf{m} \otimes J\mathbf{F}^{-T} \mathbf{n})^T \boldsymbol{\sigma} + \boldsymbol{\sigma} (\mathbf{F} \mathbf{m} \otimes J\mathbf{F}^{-T} \mathbf{n})^T] : \mathbf{l} &\end{aligned}\quad (65)$$

Denote the  $\mathbf{m}^* \otimes \mathbf{n}^* = \mathbf{F} \mathbf{m} \otimes J\mathbf{F}^{-T} \mathbf{n}$ , the  $\boldsymbol{\mu} = \text{sym}(\mathbf{m}^* \otimes \mathbf{n}^*)$  and the  $\boldsymbol{\omega} = \text{asym}(\mathbf{m}^* \otimes \mathbf{n}^*)$ , thus

$$\dot{\sigma} : \boldsymbol{\mu} = [\mathcal{L} : \boldsymbol{\mu} + \boldsymbol{\omega} \boldsymbol{\sigma} - \boldsymbol{\sigma} \boldsymbol{\omega}] : \mathbf{l} \quad (66)$$

Eq. 66 is the Hooke's law of the Schmid stress rate  $\dot{\tau}_{mn}$  and the strain rate.

Furthermore, the substitution of Eq. 63 into Eq. 61 using the elastic moduli transformation,

$$\begin{aligned}\dot{\tau}_n^m &= \dot{\mathbf{M}} : \mathbf{m}^\alpha \otimes \mathbf{n}^\alpha \\ &= [\mathcal{L} : \mathbf{l} + \boldsymbol{\sigma} \text{Tr}(\mathbf{l})] : \mathbf{F} \mathbf{m}^\alpha \otimes \mathbf{F}^{-T} J \mathbf{n}^\alpha\end{aligned}\quad (67)$$

Taking the term  $[\dot{\sigma} + \boldsymbol{\sigma} \text{Tr}(\mathbf{D}) + \mathbf{D} \boldsymbol{\sigma} - \boldsymbol{\sigma} \mathbf{D}]$  equals the term  $[\mathcal{L} : \mathbf{l} + \boldsymbol{\sigma} \text{Tr}(\mathbf{l})]$ , the Cauchy stress-strain rate is

$$\dot{\sigma} = \mathcal{L} : \mathbf{l} + \boldsymbol{\sigma} \text{Tr}(\mathbf{l} - \mathbf{D}) + \boldsymbol{\sigma} \mathbf{D} - \mathbf{D} \boldsymbol{\sigma} \quad (68)$$

The Jaumann rate of Cauchy stress is

$$\begin{aligned}\check{\sigma} &= \mathcal{L} : \mathbf{l} + \boldsymbol{\sigma} \mathbf{D} - \mathbf{D} \boldsymbol{\sigma} - \boldsymbol{\sigma} \mathbf{W} + \mathbf{W} \boldsymbol{\sigma} \\ &= \mathcal{L} : \mathbf{l} + \boldsymbol{\sigma} (\mathbf{D} - \mathbf{W}) - (\mathbf{D} - \mathbf{W}) \boldsymbol{\sigma}\end{aligned}\quad (69)$$

In terms of the total shear strains  $\mathbf{L} = \sum_{\alpha=1}^N \dot{\gamma}^\alpha \mathbf{m}^\alpha \otimes \mathbf{n}^\alpha$ ,  $\mathbf{D} = \sum_{\alpha=1}^N \boldsymbol{\mu}^\alpha \dot{\gamma}^\alpha$  and  $\mathbf{W} = \sum_{\alpha=1}^N \boldsymbol{\omega}^\alpha \dot{\gamma}^\alpha$ , the Jaumann rate of Cauchy stress with respect to the shear strains,

$$\check{\boldsymbol{\sigma}} = \mathcal{L} : \dot{\boldsymbol{\epsilon}} - \sum_{\alpha=1}^N [\mathcal{L} : \boldsymbol{\mu}^\alpha - \boldsymbol{\sigma} \boldsymbol{\omega}^\alpha + \boldsymbol{\omega}^\alpha \boldsymbol{\sigma}] \dot{\gamma}^\alpha \quad (70)$$

where the elastic strain rate  $\mathbf{l} = \dot{\boldsymbol{\epsilon}} - \sum_{\alpha=1}^N \boldsymbol{\mu}^\alpha \dot{\gamma}^\alpha$  is used because the viscous stress-shear strain rate coupling shall be excluded from the total strain rate to apply the Hooke's law. Eq. 66 is therefore

$$\begin{aligned} \dot{\tau}_{mn}^\alpha &= \dot{\boldsymbol{\sigma}} : \boldsymbol{\mu}^\alpha \\ &= [\mathcal{L} : \boldsymbol{\mu}^\alpha + \boldsymbol{\omega}^\alpha \boldsymbol{\sigma} - \boldsymbol{\sigma} \boldsymbol{\omega}^\alpha] : \left( \dot{\boldsymbol{\epsilon}} - \sum_{\beta=1}^N \boldsymbol{\mu}^\beta \dot{\gamma}^\beta \right) \end{aligned} \quad (71)$$

## VI. SINGLE CRYSTAL PLASTICITY FINITE ELEMENT PROGRAM

The crystal plasticity modeling in Huang [18] has the following constitutive equations,

- viscoplastic power-law  $\dot{\gamma}^{(\alpha)} = \dot{\gamma}^{(\alpha)}(\tau^{(\alpha)}, g^{(\alpha)})$ .
- strain hardening function  $\dot{g}^{(\alpha)} = \dot{g}^{(\alpha)}(\gamma, \dot{\gamma}^{(\beta)})$ .
- Schmid stress rate:  $\dot{\boldsymbol{\tau}}^{(\alpha)} = [\mathcal{L} : \boldsymbol{\mu}^{(\alpha)} + \boldsymbol{\omega}^{(\alpha)} \boldsymbol{\sigma} - \boldsymbol{\sigma} \boldsymbol{\omega}^{(\alpha)}] : \mathbf{D}^{\text{el}}$ .
- Jaumann rate of Cauchy stress  $\check{\boldsymbol{\sigma}} = (\mathcal{L} - \boldsymbol{\sigma} \otimes \mathbf{I}) : \mathbf{D}^{\text{el}}$ .
- lattice rotation  $\dot{\mathbf{s}}^{*(\alpha)} = \mathbf{L}^{\text{el}} \mathbf{s}^{*(\alpha)} = (\mathbf{D}^{\text{el}} + \boldsymbol{\Omega}^{\text{el}}) \mathbf{s}^{*(\alpha)}$ ,  $\dot{\mathbf{m}}^{*(\alpha)} = -\mathbf{m}^{*(\alpha)} \cdot \mathbf{L}^{\text{el}}$ .

Here, the elastic spin term  $\mathbf{W}^{\text{el}}$  in the lattice rotation is approximated by the rigid rotation rate  $\boldsymbol{\Omega}^{\text{el}} = \dot{\mathbf{R}} \mathbf{R}^{-1}$ .

During a time step  $\Delta t$ , these equations have the following incremental relations where the update parameter  $\theta$  for the forward and backward Euler methods is used for the shear strain increment  $\Delta\gamma^{(\alpha)} = \gamma^{(\alpha)}(t + \Delta t) - \gamma^{(\alpha)}(t) = \Delta t \left[ (1 - \theta)\dot{\gamma}_t^{(\alpha)} + \theta\dot{\gamma}_{t+\Delta t}^{(\alpha)} \right]$ .

The incremental shear strain

$$\Delta\gamma^{(\alpha)} = \Delta t \left[ \dot{\gamma}_t^{(\alpha)} + \theta \frac{\partial \dot{\gamma}^{(\alpha)}}{\partial \tau^{(\alpha)}} \Delta\gamma^{(\alpha)} + \theta \frac{\partial \dot{\gamma}^{(\alpha)}}{\partial g^{(\alpha)}} \Delta g^{(\alpha)} \right] \quad (72)$$

The incremental hardening function

$$\Delta g^{(\alpha)} = \sum_{\beta} h_{\alpha\beta} \Delta\gamma^{(\beta)} + \sum_{\eta} \frac{dh_{\alpha\eta}}{d\gamma^{(\beta)}} \gamma^{(\eta)} \Delta\gamma^{(\beta)} \quad (73)$$

The incremental resolved shear stress

$$\Delta\tau^{(\alpha)} = \left[ L_{ijkl} \mu_{kl}^{(\alpha)} + \omega_{ik}^{(\alpha)} \sigma_{jk} + \omega_{jk}^{(\alpha)} \sigma_{ik} \right] \cdot \left[ \Delta\epsilon_{ij} - \sum_{\beta} \mu_{ij}^{(\beta)} \Delta\gamma^{(\beta)} \right] \quad (74)$$

The corotational stress increments

$$\Delta\sigma_{ij} = L_{ijkl}\Delta\varepsilon_{kl} - \sigma_{ij}\Delta\varepsilon_{kk} - \sum_{\alpha} \left[ L_{ijkl}\mu_{kl}^{(\alpha)} + \omega_{ik}^{(\alpha)}\sigma_{jk} + \omega_{jk}^{(\alpha)}\sigma_{ik} \right] \Delta\gamma^{(\alpha)} \quad (75)$$

The increments of shear strain  $\Delta\gamma^{(\alpha)}$  (Eq. 72) in terms of given strain increments  $\Delta\varepsilon_{ij}$

$$\begin{aligned} & \sum_{\beta} \left\{ \delta_{\alpha\beta} + \theta\Delta t \frac{\partial\dot{\gamma}^{(\alpha)}}{\partial\tau^{(\alpha)}} \left[ L_{ijkl}\mu_{kl}^{(\alpha)} + \omega_{ik}^{(\alpha)}\sigma_{jk} + \omega_{jk}^{(\alpha)}\sigma_{ik} \right] \mu_{ij}^{(\beta)} - \theta\Delta t \frac{\partial\dot{\gamma}^{(\alpha)}}{\partial g^{(\alpha)}} h_{\alpha\beta} \text{sign}(\dot{\gamma}_t^{(\beta)}) \right\} \Delta\gamma^{(\beta)} \\ &= \dot{\gamma}_t^{(\alpha)} + \theta\Delta t \frac{\partial\dot{\gamma}^{(\alpha)}}{\partial\tau^{(\alpha)}} \left[ L_{ijkl}\mu_{kl}^{(\alpha)} + \omega_{ik}^{(\alpha)}\sigma_{jk} + \omega_{jk}^{(\alpha)}\sigma_{ik} \right] \Delta\varepsilon_{ij} \end{aligned} \quad (76)$$

The lattice increments

$$\Delta s_i^{*(\alpha)} = \left\{ \Delta\varepsilon_{ij} + \Omega_{ij}\Delta t - \sum_{\beta} \left[ \mu_{ij}^{(\beta)} + \omega_{ij}^{(\beta)} \right] \Delta\gamma^{(\beta)} \right\} s_j^{*(\alpha)} \quad (77)$$

$$\Delta m_i^{*(\alpha)} = -m_j^{*(\alpha)} \left\{ \Delta\varepsilon_{ij} + \Omega_{ij}\Delta t - \sum_{\beta} \left[ \mu_{ij}^{(\beta)} + \omega_{ij}^{(\beta)} \right] \Delta\gamma^{(\beta)} \right\} \quad (78)$$

The iterations are converged by the shear strain criterion

$$\Delta\gamma^{(\alpha)} - (1 - \theta)\Delta t\dot{\gamma}_t^{(\alpha)} - \theta\Delta t\dot{\gamma}_t^{(\alpha)}(\tau_t^{(\alpha)} + \Delta\tau^{(\alpha)}, g_t^{(\alpha)} + \Delta g^{(\alpha)}) = 0 \quad (79)$$

In addition, the instantaneous elastic moduli of a slip system is transferred from the global coordinate system  $\mathbf{e}$  to local coordinate system  $\check{\mathbf{e}}$  by material orientation  $\mathbf{R}$ . In terms of direction cosines,

$$\mathbf{R} = \begin{bmatrix} l_1 = \cos(e_x, \check{e}_r); & m_1 = \cos(e_y, \check{e}_r); & n_1 = \cos(e_z, \check{e}_r); \\ l_2 = \cos(e_x, \check{e}_s); & m_2 = \cos(e_y, \check{e}_s); & n_2 = \cos(e_z, \check{e}_s); \\ l_3 = \cos(e_x, \check{e}_t); & m_3 = \cos(e_y, \check{e}_t); & n_3 = \cos(e_z, \check{e}_t); \end{bmatrix} \quad (80)$$

Consider the Hooke's law in the stress-strain relation, the fourth-order material matrix in Voigt's notation from global Cartesian coordinate system  $\mathbf{e}$  to local coordinate system  $\check{\mathbf{e}}$  is expressed as

$$\mathbf{Q} = \begin{bmatrix} l_1^2 & m_1^2 & n_1^2 & 2m_1n_1 & 2l_1n_1 & 2l_1m_1 \\ l_2^2 & m_2^2 & n_2^2 & 2m_2n_2 & 2l_2n_2 & 2l_2m_2 \\ l_3^2 & m_3^2 & n_3^2 & 2m_3n_3 & 2l_3n_3 & 2l_3m_3 \\ l_2l_3 & m_2m_3 & n_2n_3 & m_2n_3 + n_2m_3 & l_2n_3 + n_2l_3 & l_2m_3 + m_2l_3 \\ l_1l_3 & m_1m_3 & n_1n_3 & m_1n_3 + n_1m_3 & l_1n_3 + n_1l_3 & l_1m_3 + m_1l_3 \\ l_1l_2 & m_1m_2 & n_1n_2 & m_1n_2 + n_1m_2 & l_1n_2 + n_1l_2 & l_1m_2 + m_1l_2 \end{bmatrix} \quad (81)$$

The elastic moduli  $C_{ijkl}$  in Voigt's notation transferred from local coordinate system to global Cartesian coordinate system,

$$\mathcal{L} = \mathbf{Q}^T \mathbb{C} \mathbf{Q} \quad (82)$$

The elastic moduli  $\mathcal{L}$  is different with the Jaumann type  $\mathcal{L} = \mathcal{C} - \boldsymbol{\sigma} \otimes \mathbf{I}$ . In practice, the difference is negligible in that the elastic moduli used unit Gpa whereas the stress used unit Mpa.

Conversely, the Cauchy stress transferred from global Cartesian coordinate system to local coordinate system by

$$\boldsymbol{\sigma}_u = \mathbf{R} \boldsymbol{\sigma} \mathbf{R}^T \quad (83)$$

If the local coordinates are aligned with the slip system  $\alpha$  for instance, the corotated Cauchy stress  $\boldsymbol{\sigma}_u$  in Voigt's notation will transform to the Schmid stress by

$$\boldsymbol{\sigma}_u^{(\alpha)} = \mathbf{Q} \boldsymbol{\sigma}_u \quad (84)$$

It is noted that the corotated Cauchy stress is symmetric and the Schmid stress is also symmetric.

As an example, a two-dimensional case is illustrated by assuming the orientation matrix

$$\mathbf{R} = \begin{pmatrix} \cos \theta & \sin \theta \\ -\sin \theta & \cos \theta \end{pmatrix}$$

and the Cauchy stress

$$\boldsymbol{\sigma} = \begin{pmatrix} \sigma_x & \tau_{xy} \\ \tau_{xy} & \sigma_y \end{pmatrix}$$

The substitution to Eq. 84 using the  $\mathbf{Q}$  matrix gives the Mohr's circle.

$$\begin{aligned} \sigma_n &= \frac{1}{2} (\sigma_x + \sigma_y) + \frac{1}{2} (\sigma_x - \sigma_y) \cos 2\theta + \tau_{xy} \sin 2\theta \\ \tau_{nm} &= -\frac{1}{2} (\sigma_x - \sigma_y) \sin 2\theta + \tau_{xy} \cos 2\theta \\ \sigma_m &= \frac{1}{2} (\sigma_x + \sigma_y) - \frac{1}{2} (\sigma_x - \sigma_y) \cos 2\theta - \tau_{xy} \sin 2\theta \end{aligned}$$

Obviously, the Cauchy stress  $\boldsymbol{\sigma} = [\sigma_x, \sigma_y, \tau_{xy}]$  is symmetric and the Schmid stress  $\boldsymbol{\sigma}^{(\theta)} = [\sigma_n, \sigma_m, \tau_{nm}]$  is also symmetric. The pressure and shear  $[\sigma_n, \tau_{nm}]$  are taken as axes of Mohr's circle.

The spin term  $\Omega_{ij}$  in Eq. 77 and Eq. 78 is obtained by the central scheme approximation

$$\frac{1}{2} \boldsymbol{\Omega} \Delta t = (\Delta \mathbf{R} - \mathbf{I}) (\Delta \mathbf{R} + \mathbf{I})^{-1} \quad (85)$$

Unambiguously, the antisymmetric part of Schmid factor  $\boldsymbol{\omega}^{(\alpha)}$  has off-diagonal terms

$$\boldsymbol{\omega} = \begin{bmatrix} 0 & \omega_{12}^{(\alpha)} & -\omega_{31}^{(\alpha)} \\ -\omega_{12}^{(\alpha)} & 0 & \omega_{23}^{(\alpha)} \\ \omega_{31}^{(\alpha)} & -\omega_{23}^{(\alpha)} & 0 \end{bmatrix} \quad (86)$$

Thus the  $\boldsymbol{\omega}^{(\alpha)} \boldsymbol{\sigma}$  term in Eq. 74

$$\boldsymbol{\omega}^{(\alpha)} \boldsymbol{\sigma} = \begin{bmatrix} \omega_{12}^{(\alpha)} \sigma_{12} - \omega_{31}^{(\alpha)} \sigma_{13} & \omega_{12}^{(\alpha)} \sigma_{22} - \omega_{31}^{(\alpha)} \sigma_{23} & \omega_{12}^{(\alpha)} \sigma_{23} - \omega_{31}^{(\alpha)} \sigma_{33} \\ -\omega_{12}^{(\alpha)} \sigma_{11} + \omega_{23}^{(\alpha)} \sigma_{13} & -\omega_{12}^{(\alpha)} \sigma_{12} + \omega_{23}^{(\alpha)} \sigma_{23} & -\omega_{12}^{(\alpha)} \sigma_{13} + \omega_{23}^{(\alpha)} \sigma_{33} \\ \omega_{31}^{(\alpha)} \sigma_{11} - \omega_{23}^{(\alpha)} \sigma_{12} & \omega_{31}^{(\alpha)} \sigma_{12} - \omega_{23}^{(\alpha)} \sigma_{22} & \omega_{31}^{(\alpha)} \sigma_{13} - \omega_{23}^{(\alpha)} \sigma_{23} \end{bmatrix} \quad (87)$$

and the symmetric part of the term  $\boldsymbol{\omega}^{(\alpha)}\boldsymbol{\sigma} + (\boldsymbol{\omega}^{(\alpha)}\boldsymbol{\sigma})^T$  in Eq. 76

$$\text{sym} \left[ \boldsymbol{\omega}^{(\alpha)}\boldsymbol{\sigma} + (\boldsymbol{\omega}^{(\alpha)}\boldsymbol{\sigma})^T \right] = \begin{bmatrix} 2 \left( \omega_{12}^{(\alpha)}\sigma_{12} - \omega_{31}^{(\alpha)}\sigma_{13} \right) \\ 2 \left( -\omega_{12}^{(\alpha)}\sigma_{12} + \omega_{23}^{(\alpha)}\sigma_{23} \right) \\ 2 \left( \omega_{31}^{(\alpha)}\sigma_{13} - \omega_{23}^{(\alpha)}\sigma_{23} \right) \\ \omega_{31}^{(\alpha)}\sigma_{12} - \omega_{23}^{(\alpha)}\sigma_{22} - \omega_{12}^{(\alpha)}\sigma_{13} + \omega_{23}^{(\alpha)}\sigma_{33} \\ \omega_{31}^{(\alpha)}\sigma_{11} - \omega_{23}^{(\alpha)}\sigma_{12} + \omega_{12}^{(\alpha)}\sigma_{23} - \omega_{31}^{(\alpha)}\sigma_{33} \\ -\omega_{12}^{(\alpha)}\sigma_{11} + \omega_{23}^{(\alpha)}\sigma_{13} + \omega_{12}^{(\alpha)}\sigma_{22} - \omega_{31}^{(\alpha)}\sigma_{23} \end{bmatrix} \quad (88)$$

In the crystal plasticity finite element method (cpfem), the shear projected by the Schmid factor is the driving force of the shear strain rate. As we discussed before, the shear stress will easily damage the material if the amount of shear strains is not controlled. cpfem is used for the single crystal material or the materials have the anisotropic deformation such that the amount of shear strains is controlled by the crss. In the conventional  $J_2$ -flow theory, the deviatoric stress is the direction of the plastic strain rate. In contrast,  $J_2$ -flow theory is used for the polycrystals or the metal sheets have the homogeneous deformation such that the specimen is uniformly elongated. In both cases, the material orientation  $\boldsymbol{Q}$  matrix is used and the uniaxial yield strength  $\sigma_y$  and the shear yield strength  $\tau_0$  are parameters to be identified. From the multiscale point of view, the cpfem is many orders of magnitude less than the conventional FEM (e.g. nanometer versus millimeter).

The Schmid stress  $\tau^\alpha$  acted as the von Mises stress  $\sigma_v$  due to the assumption that the plastic deformation is by slips. Hence, the yield function is defined. The Schmid factor  $\boldsymbol{m} \otimes \boldsymbol{n}$  acted as the deviatoric stress component directions spanned the stress space. Hence, the flow rule is defined. The slip resistance is a function of the total plastic strains. Hence, the hardening rule is defined. The criteria of elastoplasticity finite element simulation are fulfilled.

Abaqus used another contracted notation different from the Voigt's notation (Table I).

standard convection (Voigt)	Abaqus
11 → 1	11 → 1
22 → 2	22 → 2
33 → 3	33 → 3
23 → 4	12 → 4
13 → 5	13 → 5
12 → 6	23 → 6

Table I: Contracted notation convention used by Abaqus software package [19].

Abaqus umat subroutine, to implement the material nonlinearity, has the strain increment input and requires the stress and tangent stiffness matrix outputs at least. A crucial requirement is that the stresses for the new state be accurately calculated [20]. Therefore, we used the backward Euler method  $\theta = 1$  and the Newton-Raphson iterations for the stress-strain rate integration.

## VII. UNIAXIAL TENSILE TEST

The Abaqus input file is according to Huang's one-element test setting. A copper bar with dimensions (100mm  $\times$  10mm  $\times$  10mm) is fixed at one end. Another end is subjected to the tension with magnitude 200Mpa. The material orientation is defined by the lattice vector with respect to the global Cartesian coordinates. For example, the cubic crystal directions [010] and [ $\bar{1}01$ ] represent the rotation of 45° degrees around the [010] axis. The cubic elastic moduli of FCC structures are  $c_{11} = 168400\text{Mpa}$ ,  $c_{12} = 1214\text{Mpa}$  and  $c_{44} = 754\text{Mpa}$ . Three slip systems are chosen: the primary system(111)[ $\bar{1}10$ ], the conjugate system(111)[011] and the critical system (111)[1 $\bar{1}0$ ]. For each slip system, the viscoplastic power-law parameters: the rate-sensitivity exponent  $n = 10$  and the reference strain rate  $\dot{\gamma}_0 = 0.001\text{s}^{-1}$ .

The parameters of Asaro's hardening law are listed in Table II. The Asaro's hardening law described the stage I slip for each system.

$C_{11}(\text{Mpa})$	$C_{12}(\text{Mpa})$	$C_{44}(\text{Mpa})$	$h_0(\text{Mpa})$	$\tau_s(\text{Mpa})$	$\tau_0(\text{Mpa})$	$q$	$q_1$
168400	121400	75400	541.5	109.5	60.8	1	1.4

Table II: Asaro's hardening law (Eq. 52) parameters

Fig. 12 shows the uniaxial tensile test results of a copper bar. The bar under the tension is deformed plastically until the equilibrium is achieved.

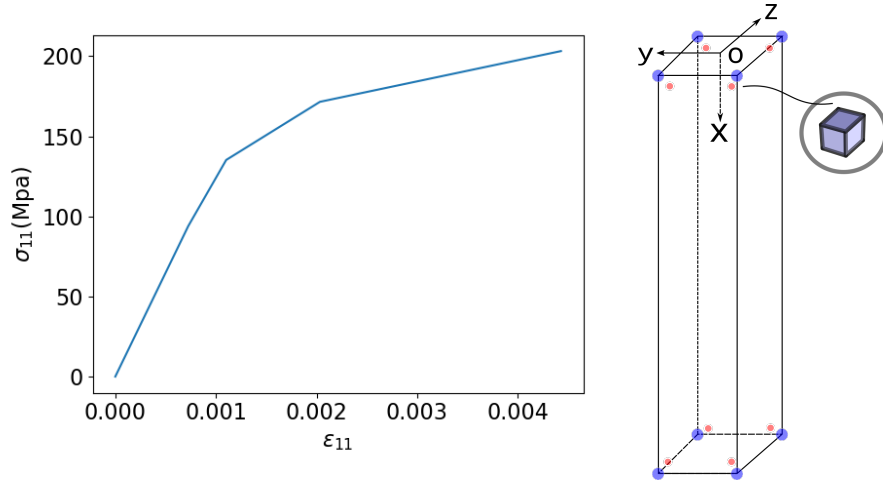
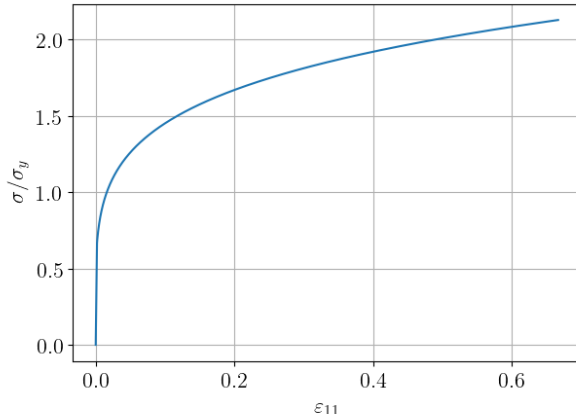


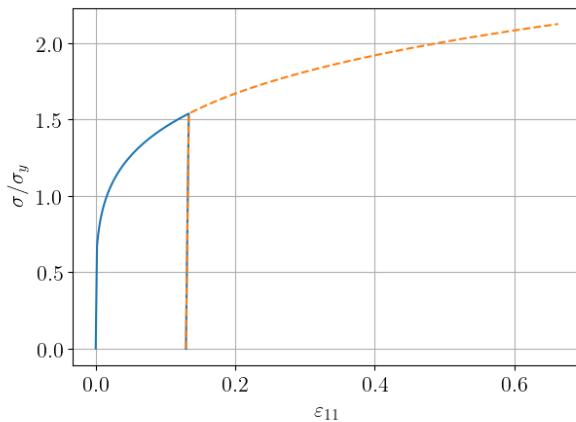
Figure 12: The uniaxial tensile test results of copper single crystal ( $\sigma_{11}$  versus  $\varepsilon_{11}(\%)$ ).

A typical stress-strain curve of uniaxial tensile test is depicted in Fig. 13, which is the integration of evolution equations in Hwang et al. [21],

$$\begin{aligned}\dot{\varepsilon}_{ij}^e &= \frac{1}{2\mu} \dot{\sigma}'_{ij} + \frac{\dot{\sigma}_{kk}}{9K} \delta_{ij} \\ \dot{\varepsilon}_{ij}^p &= \frac{3\dot{\varepsilon}^p}{2\sigma_e} \sigma'_{ij} \\ \dot{\varepsilon}^p &= \dot{\varepsilon} \left[ \frac{\sigma_e}{\sigma_y f(\varepsilon^p)} \right]^m\end{aligned}\quad (89)$$



(a)



(b)

Figure 13: 13a uniaxial stress-strain relation (Eq. 89) for rate sensitivity exponent  $m = 20$ .  $\sigma_y$  is the initial yield stress, power-law hardening exponent  $N = 0.2$ , the Young's modulus  $E = \sigma_y/0.2\%$ , Poisson's ratio  $\nu = 0.3$ . 13b loanding and unloading stress-strain curve in uniaxial tension.

where the strain is composed by the elastic and plastic part  $\varepsilon = \varepsilon^e + \varepsilon^p$ .  $\sigma_e$  is equivalent stress taken to be the von Mises stress  $\sigma_v = \sqrt{\frac{3}{2}\sigma'_{ij}\sigma'_{ij}}$  conjugate to the equivalent strain rate  $\dot{\varepsilon} = \sqrt{\frac{2}{3}\dot{\varepsilon}'_{ij}\dot{\varepsilon}'_{ij}}$ . The constitutive model of the stress-plastic strain curve in uniaxial tension is the power-law model  $\sigma = \sigma_y f(\varepsilon^p) = \sigma_y \left(1 + \frac{E\varepsilon^p}{\sigma_y}\right)^N$ .

Eq. 89 contains the hardening law, the  $J_2$ -flow rule and the yield function.  $\mu$  and  $K$  are shear and bulk modulus.  $\sigma'_{ij}$  is the deviatoric stress  $\sigma'_{ij} = \sigma_{ij} - \frac{\sigma_{kk}}{3}\delta_{ij}$ .  $\dot{\varepsilon}^p = \sqrt{\frac{2}{3}\dot{\varepsilon}_{ij}^p\dot{\varepsilon}_{ij}^p}$  is the equivalent plastic strain rate. The backward differentiation formula (bdf) method is preferred because the evolution equations are stiff.

In the macro-scale, the bar is meshed (Fig. 15 and Fig. 16). Huang's finite element program (umat) generated the stress-strain curve in Fig. 14. Instead of applying the pressure

at one end, the displacement 0.5mm is specified as a boundary condition. At the other end of bar, the pinned boundary condition is modified to be the symmetric boundary condition i.e. Z-SYMM in this case. In this boundary condition setting, the bar is uniformly elongated and the yielding is observed from Fig. 14.

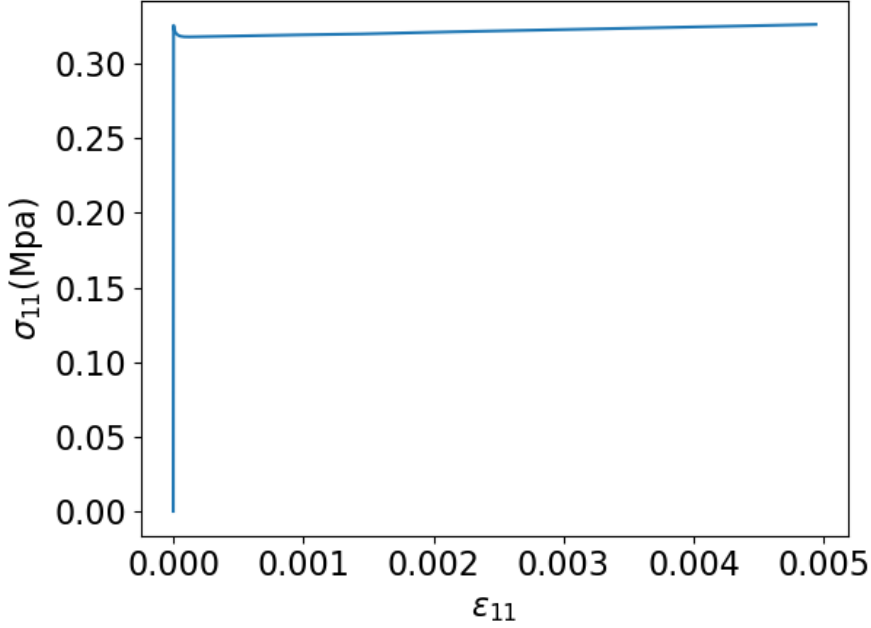


Figure 14: The stress-strain curve of an elongated bar using the material model in Table II.

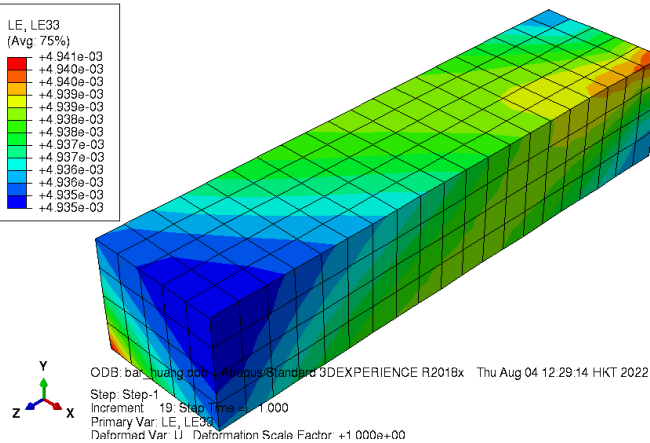


Figure 15: The strain contour plot of a deformed bar

## VIII. SUMMARY

We summarized Huang's crystal plasticity finite element program (umat) using the tensor notations. The ode methods for the constitutive equations were referenced here in the

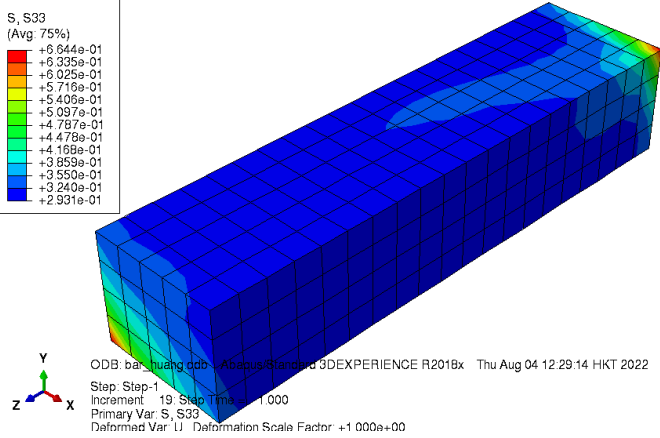


Figure 16: The stress contour plot of a deformed bar

uniaxial tensile case. Although both results are admissible, we prefer the ode methods in that it is more simple for the material parameter calibration. In comparison, the crystal plasticity constitutive equations could be simplified. For a slip system ( $\alpha$ ), we knew that

$$\begin{aligned}\dot{\gamma}_{mn}^e &= [\mathcal{L} : \boldsymbol{\mu}^\alpha + \boldsymbol{\omega}^\alpha \boldsymbol{\sigma} - \boldsymbol{\sigma} \boldsymbol{\omega}^\alpha]^{-1} : \dot{\tau}_{mn}^\alpha \quad \text{Eq. 71} \\ \dot{\gamma}_{mn}^\alpha &= \left[ H_{\alpha\beta}^{-1} \dot{g}^\beta \right] (\gamma, \gamma^\beta, \dots) \quad \text{Eq. 51} \\ \dot{\gamma} &= \sum_{\beta=1}^N |\dot{\gamma}^\beta| \quad \text{Eq. 50}\end{aligned}\tag{90}$$

Eqs. 90 are the stress-strain odes of the slip system  $\alpha$ . For metals, the lattice rotation is excluded and the rate-sensitivity part of slip resistance  $g^\alpha$  is also excluded, one is because the slip system rotation is negligible another is because the viscoplastic power-law is the smoothing of the constitutive law. Thus, the constitutive equations in terms of conventional notations are

$$\begin{aligned}\dot{\varepsilon}_{ij}^e &= S_{ijkl} \dot{\sigma}_{kl} \\ \dot{\varepsilon}_{ij}^p &= \sum_{\beta=1}^N \dot{\gamma}^\beta \mu_{ij}^\beta \\ \dot{\gamma} &= \sum_{\beta=1}^N |\dot{\gamma}^\beta|\end{aligned}\tag{91}$$

where  $S_{ijkl} = C_{ijkl}^{-1}$  is the compliance matrix and  $\mu_{ij}^\beta$  is the symmetric part of Schmid factor, e.g.  $\tau^\beta = \sigma_{ij} \mu_{ij}^\beta$ . The crystal plasticity model  $\dot{\gamma}^\alpha = H_{\alpha\beta}^{-1}(\gamma) \dot{\tau}^\beta$  is used implicitly. We demonstrated here the Asaro's model in the tension test and the Bassani-Wu's model in the shear test.

The parameters we chosen for the Asaro's model are listed in Table III where the active slip systems are the primary system  $(1\bar{1}\bar{1})[101]$ ,  $(1\bar{1}\bar{1})[0\bar{1}\bar{1}]$  and the critical system  $(111)[1\bar{1}0]$ . In Fig. 17, the Asaro's model reveals the gliding behavior of a single slip, which explains the physical mechanism of the initial yielding of the bulk crystal. The Bassani-Wu's model

$h_0$ (Mpa)	$\tau_0$ (Mpa)	$\tau_s$ (Mpa)	$q$	$q_l$
1.0	1.0	2.0	1	1.4

Table III: Asaro's hardening law (Eq. 52) parameters (plastic only)

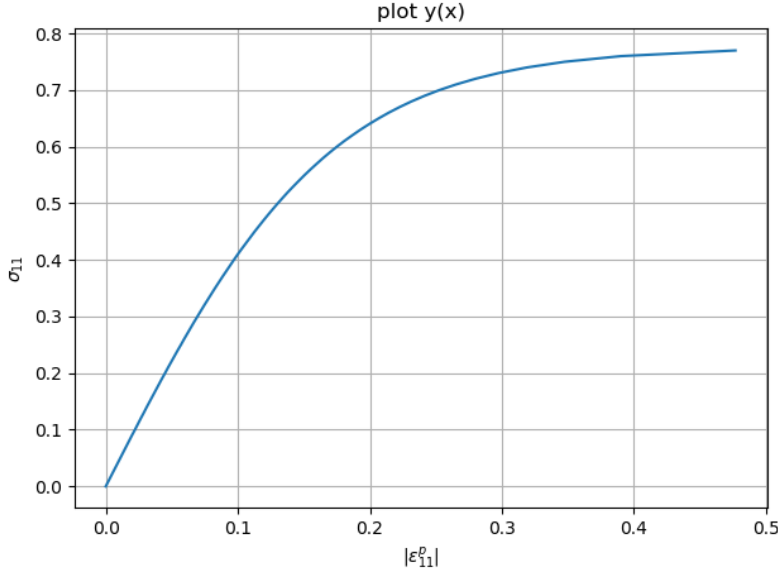


Figure 17: The uniaxial tensile plot ( $\sigma_{11} - |\epsilon_{11}^p|$ ) of Asaro's model using parameters in Table III

$h_0$ (Mpa)	$\tau_0$ (Mpa)	$\tau_s$ (Mpa)	$h_s$ (Mpa)	$q$	$q_l$
1.0	1.0	2.0	0.01	1	1.4

Table IV: Bassani-Wu's hardening law (Eq. 53) parameters (plastic only)

further included the anisotropic latent effects whose parameters are listed in Table IV and its shear stress plot is Fig. 18. The active slip systems are the primary system  $(11\bar{1})[101]$ ,  $(11\bar{1})[0\bar{1}\bar{1}]$  and the critical system  $(111)[\bar{1}01]$ .

Both the Asaro's model and the Bassani-Wu's model correspond to the experimental evidence in Maass et al. [23] and [22] (see Fig. 19 and Fig. 20). Using the material parameters determined by the experiments, the cpfem simulation will be accurate.

- [1] M. Wang and P. D. Eggenschwiler, Modeling of three way catalyst behavior under steady and transient operations in a stoichiometric natural gas fueled engine, in, SAE Tech. Pap. Ser , 1 (2021).
- [2] Y. Zhu, K. Ameyama, P. M. Anderson, I. J. Beyerlein, H. Gao, H. S. Kim, E. Lavernia, S. Mathaudhu, H. Mughrabi, R. O. Ritchie, et al., Heterostructured materials: superior properties from hetero-zone interaction, Materials Research Letters 9, 1 (2021).
- [3] L. Zhu and J. Lu, Modelling the plastic deformation of nanostructured metals with bimodal

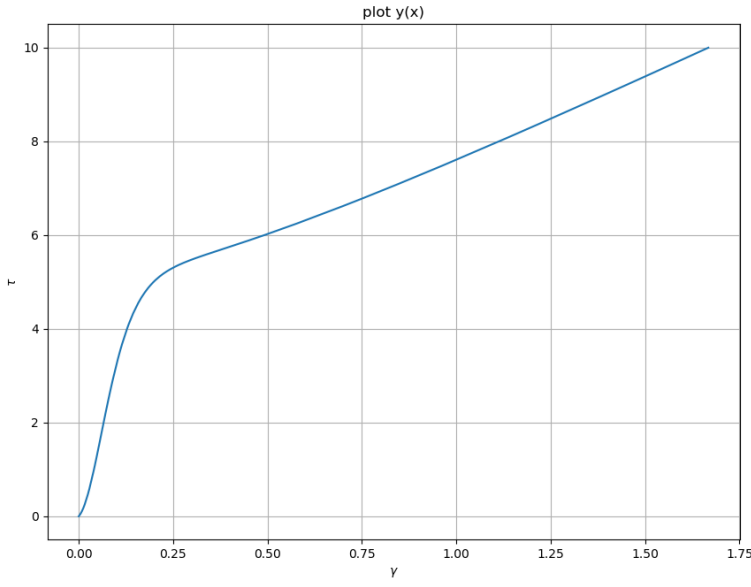


Figure 18: The shear stress plot ( $\sigma_{23} - \varepsilon_{23}^p$ ) of Bassani-Wu's model using paramters in Table IV

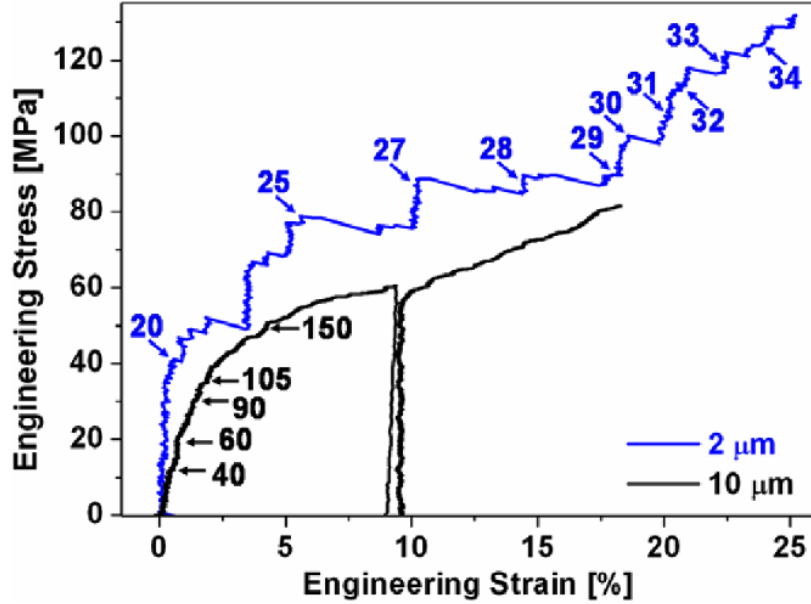


Figure 19: Maass et al. [22] shows the size effect of micropillar compression.

grain size distribution, International Journal of Plasticity 30, 166 (2012).

- [4] K. Ameyama, F. Cazes, H. Couque, G. Dirras, S. Kikuchi, J. Li, F. Mompiou, K. Mondal, D. Orlov, B. Sharma, et al., Harmonic structure, a promising microstructure design, Materials Research Letters 10, 440 (2022).
- [5] H. Gao and Y. Huang, Geometrically necessary dislocation and size-dependent plasticity, Scripta Materialia 48, 113 (2003).
- [6] M. Ashby, The deformation of plastically non-homogeneous materials, The Philosophical Mag-

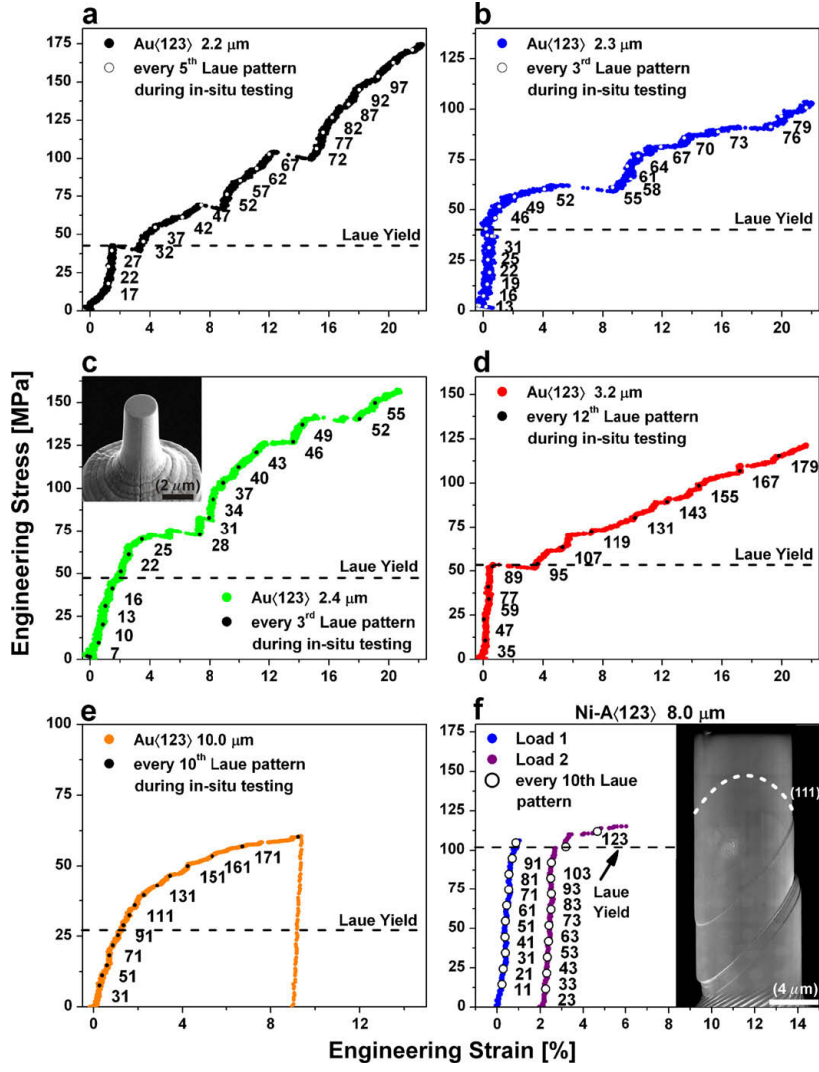


Figure 20: Maass et al. [23] concludes that the size effect of micropillar follows the "Smaller is stronger." principle.

- azine: A Journal of Theoretical Experimental and Applied Physics 21, 399 (1970).
- [7] G. I. Taylor, Plastic strain in metals, J. Inst. Metals 62, 307 (1938).
  - [8] H. Mughrabi, On the role of strain gradients and long-range internal stresses in the composite model of crystal plasticity, Materials Science and Engineering: A 317, 171 (2001).
  - [9] M. Peach and J. Koehler, The forces exerted on dislocations and the stress fields produced by them, Physical Review 80, 436 (1950).
  - [10] J. P. Hirth and J. Lothe, Theory of dislocations (John Wiley & Sons, 1982).
  - [11] J. Cheng, H. J. Bong, H. Qiao, X. Hu, X. Sun, S. Ghosh, and P. Wu, Comparison of three state-of-the-art crystal plasticity based deformation twinning models for magnesium alloys, Computational Materials Science 210, 111480 (2022).
  - [12] C. Kords and D. Raabe, On the role of dislocation transport in the constitutive description of crystal plasticity (epubli GmbH Berlin, 2013).
  - [13] F. Mouhat and F.-X. Coudert, Necessary and sufficient elastic stability conditions in various crystal systems, Physical review B 90, 224104 (2014).

- [14] T. Belytschko, W. K. Liu, B. Moran, and K. Elkhodary, Nonlinear finite elements for continua and structures (John wiley & sons, 2014).
- [15] F. Dunne and N. Petrinic, Introduction to computational plasticity (OUP Oxford, 2005).
- [16] R. J. Asaro and A. Needleman, Overview no. 42 texture development and strain hardening in rate dependent polycrystals, *Acta metallurgica* 33, 923 (1985).
- [17] J. L. Bassani and T.-Y. Wu, Latent hardening in single crystals. ii. analytical characterization and predictions, *Proceedings of the Royal Society of London. Series A: Mathematical and Physical Sciences* 435, 21 (1991).
- [18] Y. Huang et al., A user-material subroutine incorporating single crystal plasticity in the ABAQUS finite element program (1991).
- [19] E. J. Barbero, Finite element analysis of composite materials using AbaqusTM, Vol. 2103 (CRC press Boca Raton, 2013).
- [20] K.-J. Bathe, Finite element procedures (Klaus-Jurgen Bathe, 2006).
- [21] Y. Huang, S. Qu, K. Hwang, M. Li, and H. Gao, A conventional theory of mechanism-based strain gradient plasticity, *International Journal of Plasticity* 20, 753 (2004).
- [22] R. Maaß, S. Van Petegem, H. Van Swygenhoven, P. M. Derlet, C. A. Volkert, and D. Grolimund, Time-resolved laue diffraction of deforming micropillars, *Physical review letters* 99, 145505 (2007).
- [23] R. Maaß, S. Van Petegem, D. Ma, J. Zimmermann, D. Grolimund, F. Roters, H. Van Swygenhoven, and D. Raabe, Smaller is stronger: The effect of strain hardening, *Acta Materialia* 57, 5996 (2009).